ACS Photonics

Article

pubs.acs.org/journal/apchd5

Light-Induced Field Enhancement in Nanoscale Systems from First-Principles: The Case of Polyacenes

Luca Bursi,[†,‡] Arrigo Calzolari,*[,‡] Stefano Corni,*[,‡] and Elisa Molinari[†,‡]

[†]Dipartimento di Fisica, Informatica e Matematica, Università di Modena e Reggio Emilia, I-41125 Modena, Italy

[‡]Istituto Nanoscienze CNR-NANO-S3, I-41125 Modena, Italy

Supporting Information

ABSTRACT: Using first-principles calculations we studied the electric field enhancement in polyacene molecules upon illumination. These molecules can be seen as a specific class of C-based (i.e., graphene-derived) nanostructures, recently proposed as alternative materials for plasmonics. We demonstrate that optical transitions may generate oscillating dipolar response charge, giving rise to an induced electric field near the molecule, which thus acts as a plasmon-like nanoantenna. While the field amplification in the vicinity of single acenes is rather small and decreases when the size of the system is increased, it may be selectively enhanced in the case of acene's assemblies. This paves the way for the design of more complex C-based architectures explicitly conceived to improve the amplification factor.

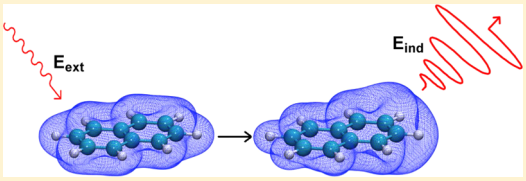

KEYWORDS: *field-enhancement, plasmonic nanoantenna, polyacenes, C-based nanostructures, TDDFT*

In nanosystems, an external electromagnetic field such as incoming light may excite localized surface plasmon resonances. This is associated with the confinement of electromagnetic energy to nanometric regions, below the diffraction limits,[1−4] which can produce a local enhancement of the external electromagnetic field near the nanosystem.[5−7] When this happens, the system acts as a plasmonic nanoantenna able to amplify local electric fields at the nanoscale. This phenomenon is particularly appealing in light harvesting devices, which require highly efficient broadband sunlight absorption and photoexcitation, particularly in the visible and near-IR wavelengths,[8] energy conversion,[9] and telecommunications[10] in the terahertz (THz) region. Plasmonic nanosensors have been proposed for biomedical applications,[11,12] where they allow spectroscopy in truly nanometer-scale volumes, increasing signals and resolution of surface-enhanced spectroscopies[13−15] up to single-molecule sensing.[16,17] Also, nanoplasmonics has raised the general interest in the possibility of merging the compactness of nanoelectronics and the speed of photonics.[18−22]

Noble metal nanoparticles are the nanoplasmonics materials *par excellence*, and their intriguing optical properties have been exploited for centuries.[23] On the theoretical side, the microscopic study of those effects is a major challenge. In macroscopic systems, the key physical quantity that governs these phenomena is the complex frequency-dependent dielectric function. This quantity is generally well described by the semiclassical Drude−Lorentz model that provides experimentally verifiable expressions of the optical properties of the systems, in their bulk phase, in terms of intraband transitions.[24]

Moving to the nanoscale, the dielectric function is dependent on the size and on the shape of the system.[25,26] When the system size reaches a few nanometers, the density of state changes from a continuum to a discrete set of levels, underlining the molecular character of these nanostructures and the quantum nature of their excitations.[27−30] In particular, the way the excitation properties of molecules transform into that of nanostructures and then into macroscopic bulk is far from being understood, and it is a field of current debate.[31−36]

Carbon-based nanostructures, such as graphene nanoribbons and nanoflakes, have emerged as nanoplasmonic materials,[37−41] alternative to standard metallic systems (e.g., Au, Ag). Graphene plasmons possess high frequency tunability, long excitation lifetimes, reduced loss, and larger oscillator strength compared to noble metals or two-dimensional electron gas (2DEG).[42,43] The promising plasmonic properties of graphene and its nanostructures have been demonstrated in the past few years by means of various experimental techniques,[44−48] widening the large range of extraordinary properties displayed by this unique one-atom-thick material.[49] Graphene nanostructures present, however, the same conceptual difficulties as for metal nanoparticles in understanding the intermediate regime between molecule and bulk.[50−53]

Within this work we consider a set of polyacenes,[54] i.e., polycyclic aromatic hydrocarbons (PAHs) composed of a single linear chain of condensed benzene rings. PAHs have been largely studied due to their environmental impact,[55] their role as carcinogens,[56] and their applications in astrophysics[57−60] and in organic optoelectronics devices.[61,62] Polyacenes can also be seen as constituent building blocks of zigzag graphene nanostructures (e.g., nanoflakes).[63,64]

Received: July 24, 2014
Published: September 24, 2014

   dx.doi.org/10.1021/ph500269q | *ACS Photonics* 2014, 1, 1049−1058

A wide number of theoretical works have investigated the optical properties of such molecules with a broad range of theoretical methods.[65−69] In particular, García de Abajo et al.[52] have studied different classes of PAHs, by means of a time-dependent density functional theory (TDDFT) approach, finding that they exhibit collective electronic excitations with an intrinsic quantum nature, which can be referred to as "molecular plasmons". They demonstrated that plasmons of PAHs exhibit an exceptional structural (edge states are extremely important) and electrical tunability, even greater than graphene, allowing to be switched on/off by addition or removal of a single electron. At the same time, Guidez et al.[53] identified the main peak in the low-energy region of the acenes' spectra as the molecular plasmon peak considering the induced density shape and on the basis of a configuration interaction approach for naphthalene.

Due to the ambiguities in the definition of plasmons at the molecular scale, here we prefer to focus on a typical plasmonic effect, i.e., the electric field enhancement. We consider purely molecular systems that exhibit interband optical transitions upon interaction with light. These transitions may cooperate constructively, in a collective way (i.e., with comparable weights), leading to relatively intense absorption peaks, which can be considered "plasmonic" since they may enhance an external electric field.[36,53]

More specifically, we take into account polyacenes with a number of rings between 1 and 5 and the 50-acene. Their electronic and optical absorption properties and the local electric field enhancement near these systems are investigated through first-principles (TD)DFT approaches,[70,71] with particular focus on their scaling with respect to the size of the system. We finally investigate the field amplification effect due to light excitation of pairs of acences (naphthalenes) at different distances. Our results show a small but not negligible field enhancement cooperation effect between molecules. This proof of concept suggests that, even though the amplification properties of single acenes are generally too small for any realistic application, their supramolecular coupling may provide a tunable and controlled way to realize realistic nanoantenna.

METHODS

First-principles simulations of electronic structures and absorption spectra have been carried out by using the QUANTUM ESPRESSO[70] (QE) suite of codes, based on density-functional theory (DFT). We adopt the PBE[72] generalized gradient approximation (GGA) to the exchange−correlation (xc) functional. Single-particle wave functions and charge density are expanded in plane waves within an energy cutoff of 25 Ry and of 300 Ry, respectively. This representation ensures also well-converged optical spectra, as we have verified (convergence test is included in the Supporting Information (SI)).

All systems are simulated with periodically repeated supercells, each containing the molecules—set in the *xy* plane, with their long axis parallel to the *x* direction—and ∼11 Å of vacuum to separate adjacent replica in the three spatial directions. Calculations of the electronic structure are performed at the Γ point of the Brillouin zone (BZ).

The molecular structures are relaxed under the effect of the interatomic forces, with the exception of the 50-acene, whose structure is built starting from the equilibrium coordinates of pentacene. Previous DFT investigations have predicted an undistorted symmetrical structure and an antiferromagnetic coupling of unpaired electrons for polyacenes with a large number of aromatic rings (>7).[73,74] We carried out spin-resolved calculations, within local spin density approximation, of the 50-acene ground-state electronic structure, which turned out to be in agreement with that prediction, as shown by the spin polarization, reported in Figure S3 of the SI. Moreover, while for the shorter acenes taken in consideration here it does not represent a dominant effect, Jahn−Teller distortion plays a role in the case of 50-acene. However, in this context, the 50-acene represents a model system to analyze the scaling of the electronic, optical, and plasmonic properties of acenes with respect to the size of the system. Thus, in the present work, we will deal with the case of spin-restricted calculations in order to provide comparable results with the short systems considered.

For the simulation of optical absorption spectra and the response charge densities, we adopted the turboTDDFT code,[71] also distributed within the QE package, which implements a Liouville−Lanczos approach to time-dependent density functional theory. This approach is computationally very efficient in the calculation of the absorption spectra in the frequency domain and is well suited for large systems composed of hundreds of atoms.

RESULTS AND DISCUSSION

In this section we first discuss the ground-state properties of the systems under investigation; then we show the absorption spectra and the response charge densities. These charge densities are the input for the evaluation of the response electric fields, which will be the subject of the next part of the section. The results are discussed in terms of the increasing size of the molecules. Finally, we analyze the optical properties and the local field enhancement of a coupled system, composed of two coplanar naphthalene molecules, at different distances.

Ground-State Properties. We studied the ground-state properties of polyacenes composed of an increasing number (N) of conjugated rings, namely, benzene (N = 1), naphthalene (N = 2), anthracene (N = 3), tetracene (N = 4), pentacene (N = 5), and 50-acene (N = 50). Here, we report the results only for the long, not previously studied 50-acene. The electronic structures of shorter acenes ($N \leq 5$) have been largely studied and are summarized in the SI for completeness.

Figure 1 (upper panel) displays the highest occupied (HOMO) and the lowest unoccupied molecular orbital (LUMO) of the 50-acene. They exhibit a π-character and are fully distributed along the entire molecule, which is the typical fingerprint of charge conjugation in aromatic systems.[75] From

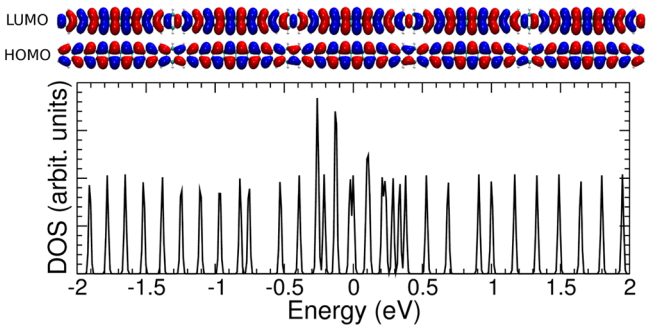

Figure 1. (Top) Isosurface plot of HOMO and LUMO states of 50-acene. (Bottom) DOS of the 50-acene, where the HOMO energy is set to zero.

dx.doi.org/10.1021/ph500269q | ACS Photonics 2014, 1, 1049−1058

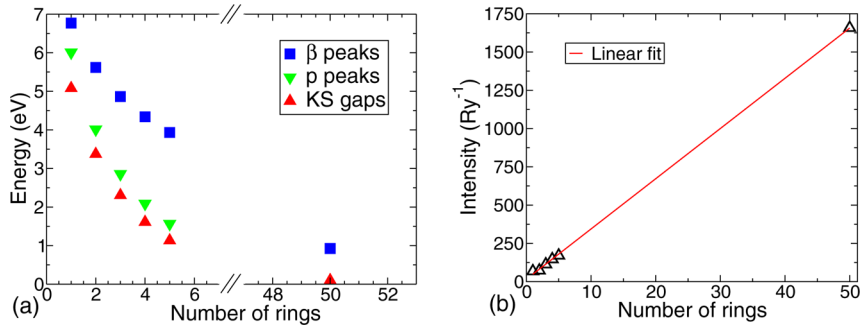

Figure 2. (a) Comparison between the KS energy gaps and the absorption edges for the systems under consideration. (b) Intensity of the β absorption peak as a function of the number of phenyl rings. Red line is the linear fit extracted from the TDDFT values.

the comparison of the states of the different molecules it can be observed that the number of nodes of the single-particle wave functions increases with the increasing number of benzene rings. However, all the HOMO states have the same kind of symmetry; that is, they are antisymmetric with respect to *xz* and *xy* planes. Moreover they are antisymmetric or symmetric with respect to the *yz* plane depending on whether they are composed of an even or an odd number of rings, respectively. This is true also for the LUMO states, which are antisymmetric with respect to *xy* and symmetric with respect to *xz* planes; furthermore they are antisymmetric or symmetric with respect to the *yz* plane depending on the number of rings. Benzene represents a peculiar system with respect to the others under study because it shows more symmetry axes; in particular it has a C_6 axis, which is missing in the other acenes.

The bottom panel of Figure 1 shows the density of states (DOS) of the 50-acene molecule.[76] As the number of benzene rings is increased, the density of occupied states increases, while the Khon−Sham (KS) HOMO−LUMO gap decreases, becoming extremely small (98 meV) in the present case and zero (i.e., metallic behavior) for the infinite (spin-unpolarized) polymer. This trend is underlined in Figure 2a, where the calculated KS gaps are plotted as a function of the number of benzene rings of the systems and are compared with the energies of the peaks calculated within a TDDFT approach (see next section for discussion).

Absorption Spectra. The TDDFT results are displayed in Figure 3, where the absorption spectra show features common to all the systems under investigation: following the classification labels proposed by Clar,[54] we identify a net sharp peak, which corresponds to the β band of the acenes (B_{3u} symmetry) and a low-intensity peak at lower energy, which is the p band (B_{2u} symmetry), in agreement with previous theoretical results.[53,68] The p peak is not observed in the case of the 50-acene. These low-energy sharp spectral features (p and β) are followed by a broad band at higher energies. While shorter molecules absorb light in the UV, the 50-acene has the absorption edge in the near-IR. We expect therefore absorption in the visible range as well for molecules with an intermediate size.

Our theoretical results well reproduce the experimental findings,[77] confirming the prediction capability of our method. From the comparison of the UV−vis spectra of different acenes we note that the intensity of the main peak β increases linearly with the number of included rings; see Figure 2b.

A similar behavior is not obviously predictable a priori, since the system could also show a sublinear or saturation trend of

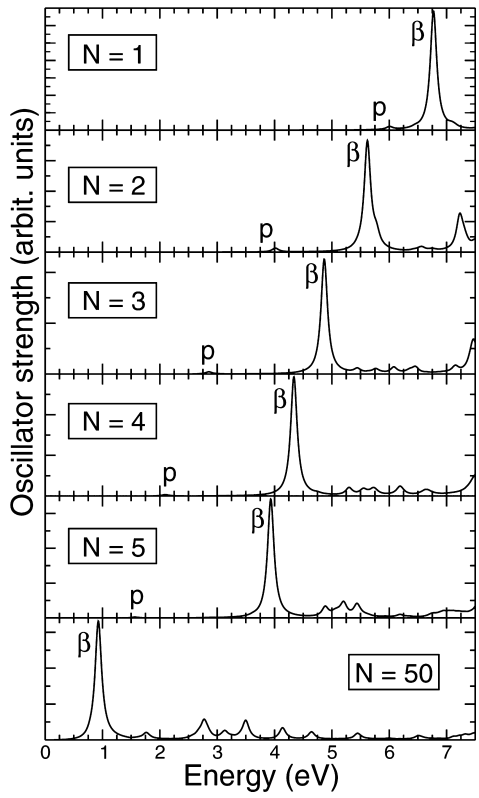

Figure 3. Absorption spectra of molecules with different numbers of aromatic rings, *N*, in the low-energy region.

the absorption. A linear fit performed on the TDDFT data (Figure 2b) gives a slope coefficient of 32.8 Ry^{-1}.

These coefficients refer to maximum intensities, but the total oscillator strength integrated on each peak also follows the same trend. Benzene represents a unique case. In fact the intensity of its β absorption peak is almost the same as that of naphthalene; thus its position in the plot of Figure 2b slightly deviates from the general trend.

The increase of the molecular size goes together with the decrease of the energies of their absorption edges. This result could be qualitatively interpreted invoking the quantum particle-in-a-box model for a one-dimensional potential well. In this model the energies of the states are expressed by the relation $\varepsilon_n \propto n^2/l^2$, where the integer number n is the index of the states and l is the width of the box. The energy difference between two consecutive energy levels is given by $\Delta\varepsilon_n \propto (2n + 1)/l^2$. Considering that n for the HOMO is proportional to the number of electrons, i.e., to the number N of rings, and that the

dx.doi.org/10.1021/ph500269q | ACS Photonics 2014, 1, 1049−1058

size of the molecule l is also trivially proportional to N, we obtain that $\Delta\varepsilon_n \propto N/N^2 \approx N^{-1}$.

The N^{-1} behavior is in qualitative agreement with the trend of the KS gaps and of the energies of the absorption peaks, reported in Figure 2a. Fitting the graphs in Figure 2a with a power function, we found that the KS energy gap decreases with the trend $N^{-1.05}$, while the energy of the TDDFT absorption p peaks decreases like $N^{-0.82}$, i.e., with a power factor significantly different from −1. Thus, the trend of single-particle gaps is consistent with the infinite potential quantum well model. On the contrary, the TDDFT results significantly deviate from this picture, indicating the inadequacy of the single-particle approach in describing even the trend of optical excitations. In Figure 2a we plot, for completeness, also the trend of the energy of the main β peak as a function of N, which is decreasing as $N^{-0.53}$, even more slowly than the p peak. It should be emphasized that, for all the acenes, the p peak is the one mainly given by the HOMO−LUMO transition.

It is well established that both KS and TDDFT gaps may suffer severe underestimations, due to the choice of the PBE xc functional. The use of a hybrid xc functional provides results closer to the experimental values,[53,67,68] but at a significantly greater computational cost when a plane-wave basis set is employed. As an accuracy test, we performed the calculation of the optical properties of tetracene exploiting a hybrid B3LYP functional.[78] The B3LYP spectrum is in good agreement with the PBE one, except for a rigid blue-shift (∼260 meV) of the absorption edge. Apart from this expected shift, the calculations with the hybrid functional confirm the results obtained at the PBE level, including the field enhancement effects described in the next section (comparison shown in the SI). Actually the response charge density obtained with the hybrid B3LYP is slightly more localized with respect to the PBE one. It is also well known that, for conjugated polymers, PBE may underestimate screening effects, yielding too large static polarizabilities.[79,80] Large improvements in this context are found[79] by using the Vignale−Kohn functional. Our conclusions are nonetheless robust with respect to this possible overestimation, especially since the B3LYP results confirm the PBE description. Although beyond the aim of this work, range-separated hybrid functionals would provide, in general, more accurate results in organic compounds than global hybrids.

Response Charge Density. In order to gain insight into the microscopic origin of the main peaks, we analyze the response charge density, which is representative of the spatial localization of the dipolar excitations induced by a homogeneous monochromatic external electric field. The specific TDDFT method we used gives a direct access to the response charge density, $n'(\omega)$, whose imaginary part is related to the absorption spectra at each frequency ω. The 3D plots of the response charge density corresponding to both β and p absorption peaks are shown in Figure 4 for naphthalene (upper panel) and 50-acene (bottom panel); the same plots for the other acenes are reported in the SI.

The electronic excitations responsible for the β peaks are due to oscillations of the electron charge density along the main axis of the molecule (x). The lower-intensity p peaks are instead originated by oscillations along the perpendicular direction (y). Out-of-plane oscillations (z direction) do not contribute with sizable oscillator strengths. Benzene represents an exception because of its D_{6h} symmetry, in agreement with the existing literature.[53,54]

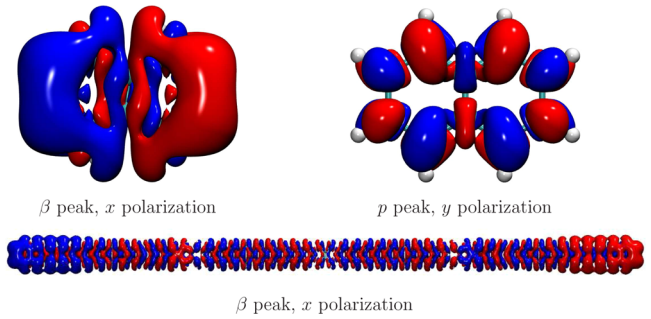

Figure 4. Isosurface plots of the imaginary part of the response charge density for naphthalene (upper panel) and 50-acene (bottom panel). The polarization of the incoming field and the peak at whose frequency the response is calculated are also indicated. Blue and red colors refer to positive and negative values of the response charge density, respectively.

The response charge density calculated at the frequency of the β peak, when the polarization of the external field is parallel to the x direction, is polarized along the main axis of the molecules and shows the clear character of a longitudinal dipole. The charge density is localized at the sides of the molecule, leaving a charge depletion in the center. This is evident for all the systems and especially in the case of 50-acene, where a long longitudinal dipole can be observed. Furthermore, due to the greater extension of the molecule along x, a net modulation of the charge density response is clearly detected at about one-fourth of the length of the molecule (Figure 4). We can conclude that the excitations of the acenes responsible for the β peaks in the absorption spectra have a major dipolar character.

From the projection of the response charge on single-particle KS orbitals for occupied (ψ_v) and empty (ψ_c) states, we can also interpret the absorption features in terms of electron−hole transitions: $n'(\mathbf{r}) = \Sigma_{vc}\xi_{vc}\Psi_c^*(\mathbf{r})\ \Psi_v(\mathbf{r})$. The results for naphthalene and 50-acene are summarized in Table 1, while the coefficients relative to other acenes are reported in the SI. The analysis of the single-particle transitions indicates that only a few groups of states (i.e., the frontier orbitals) contribute to the absorption peaks of short acenes ($N \leq 5$). In particular, in-plane x polarization of the β peak has a predominant HOMO−1 → LUMO and HOMO → LUMO+1 character in the case of naphthalene and anthracene, while HOMO−2 → LUMO and HOMO → LUMO+2 leading contributions in the case of tetracene and pentacene; benzene is peculiar because it shows more symmetry axes and because of its double-degenerate HOMO and LUMO. On the contrary, for 50-acene the number of single-particle transitions that contribute to the β peak is largely increased (around 80 single-particle transitions), giving to the excitation a "collective" character. This has been associated in the literature to a plasmonic-like behavior,[32] in analogy with bulk systems. As mentioned above, the β peaks of polyacenes have been identified as "molecular plasmons"[53] also on the basis of the response charge density appearance.[31]

This is a notable result since little is known on the way the single-particle excitations cooperate to give collective excitations in nanosystems. The understanding of the evolution of single-particle excitations of nanoscale systems to collective excitations in bulks (e.g., bulk plasmons) would be a major achievement, and it represents one of the long-term motivations of the present work.

dx.doi.org/10.1021/ph500269q | ACS Photonics 2014, 1, 1049−1058

Table 1. Main Electron−Hole Components ξ_{vc}, Normalized Such That $\Sigma_{vc}\mathrm{Im}(\xi_{vc})^2 = 1$ and Expressed in Percentage Form, of the Lowest-Energy Peaks of Selected Naphthalene and 50-Acene

naphthalene		50-acene
β peak, x polarization	p peak, y polarization	β peak, x polarization
HOMO−1 LUMO	HOMO LUMO	HOMO LUMO+1
49%	87%	10%
HOMO LUMO+1	HOMO−2 LUMO+3	HOMO−1 LUMO
47%	6.1%	8.9%
HOMO−5 LUMO+3	HOMO−1 LUMO+1	HOMO−11 LUMO+136
1.5%	4.7%	5.9%
HOMO−2 LUMO+17	HOMO−5 LUMO+17	HOMO−12 LUMO+121
0.88%	0.85%	5.6%
HOMO LUMO+22	HOMO−8 LUMO+1	HOMO−10 LUMO+121
0.35%	0.35%	4.4%

It is worth noticing that, as partially occupied bands do not exist in closed-shell molecules, intraband excitations cannot rigorously exist; thus for shorter acenes, the transitions that occur between different discrete states may be considered interband. Larger systems (such as long molecules or metallic nanoparticles) tend to assume characters closer to the bulk systems: their energy states, while remaining discrete, become denser, giving rise to band-like electronic structures. In this case, for metallic systems both intra- and interband transitions could exist. However, this is not the case either for long polyacenes. To prove this, we have drawn a parallel with the infinite (spin-unpolarized) polymer for which we calculated one-dimensional bands. The strong optical transitions, corresponding to the β band of polyacenes, are interband-like, since they occur between different bands having different symmetries. This justifies the interband attribution to optical excitations in acene systems.

Electric Field Enhancement. The large oscillator strength of the β peaks and their identification as molecular plasmons suggest the possibility that carbon-based nanosystems may act as "plasmonic antenna",[43,50] providing a local amplification of the external electromagnetic field.

The external electromagnetic field $\mathbf{E}_{ext}(\omega) = \mathbf{E}^0_{ext}e^{-i\omega t}$ excites the electronic charge density, which, as a response, oscillates, generating an *induced* electric field, given by

$$\mathbf{E}_{ind}(\mathbf{r}, t) = \int n'(\mathbf{r}', t)\frac{\mathbf{r} - \mathbf{r}'}{|\mathbf{r} - \mathbf{r}'|^3}d^3\mathbf{r}' \quad (1)$$

where $n'(\mathbf{r}', t)$ is the response charge density, which we can directly obtain from the TDDFT calculations. To simplify the notation, we dropped the ω dependence of $\mathbf{E}_{ind}$ and n'. The total field in the vicinity of the nanostructure results to be $\mathbf{E}_{ext} + \mathbf{E}_{ind}$, while the field enhancement is defined as the ratio $|\mathbf{E}_{ext} + \mathbf{E}_{ind}|/|\mathbf{E}_{ext}|$.

The total electric field plot for naphthalene in the (x, y) plane, calculated $\Delta = 3.3$ Å above the plane of the molecule, is shown in Figure 5a, and in Figure 5b the geometry of the system is schematized; plots for the other short acenes are reported in the SI. Δ has been chosen as 3.3 Å since it is a typical nonbonding distance between stacked organic molecules. In agreement with the character of the response charge, the induced electric field is consistent with an electric field generated by an oscillating dipole.

Figure 5c shows the field enhancement along the molecular axis, as illustrated in Figure 5b. The zero distance reference is taken at the center of the molecule. The maximum value of the modulus of the electric field decreases with the increase of the number of rings of the molecule (N). The modulus of the electric field calculated at the center of the molecule decreases with the increase of N.

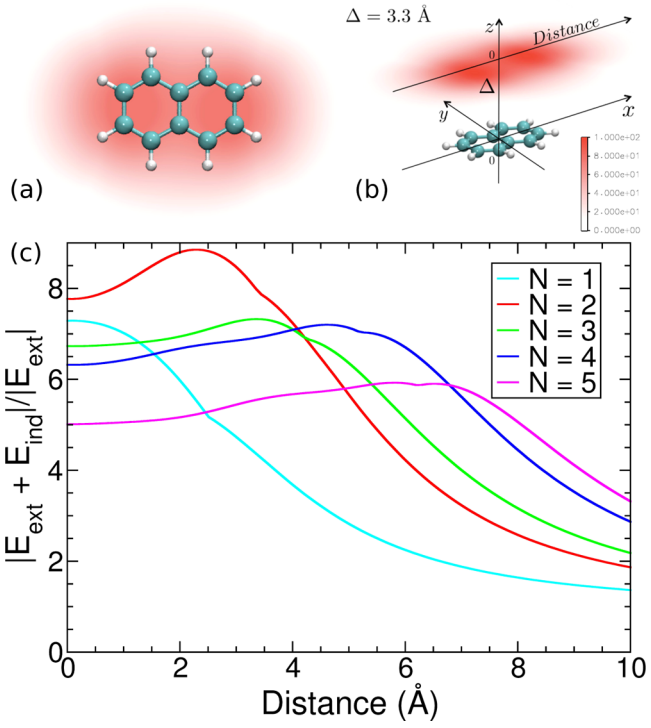

Figure 5. Top (a) and side (b) view of 2D intensity plot representation of the induced electric field in the (x, y) plane, calculated 3.3 Å above the plane of the naphthalene molecule. (c) Electric field enhancement of longitudinally polarized excitations of short acenes ($N \leq 5$), computed along the axis of the molecules, 3.3 Å above their plane. The distance indicated in the x axis refers to the distance from the center of each molecule.

This trend can be rationalized a posteriori within a simple dipole model, i.e., assuming the response charge can be modeled as two point charges $+q$ and $-q$ separated by a distance l, which is the length of the molecule. At the center of the molecule the intensity of the electric field produced by the dipole, at a distance Δ from its plane (see panel b), scales like

$$E_{ind} \approx \frac{ql}{(4\Delta^2 + l^2)^{3/2}} \quad (2)$$

At resonance, the dipole moment induced on the molecule is approximately proportional to the imaginary part of the

dx.doi.org/10.1021/ph500269q | ACS Photonics 2014, 1, 1049−1058

dynamical polarizability,[50] i.e., to the oscillator strength for a 0 → β transition ($f^{0\beta}$). Furthermore, our results indicate that the intensity of the oscillator strength $f^{0\beta}$ scales linearly with the size of the system; hence we can state that the induced dipole moment is proportional to the length of the system. In light of the above considerations, we can write eq 2 as

$$E_{ind} \propto \frac{1}{l^2\left(1 + \frac{4\Delta^2}{l^2}\right)^{3/2}} \quad (3)$$

Therefore, the electric field obtained in the middle of the molecule *decreases* with the increase of l and thus with the number of aromatic rings in the molecule. The maximum of the response field tends to be centered at the edges of the molecules, where the response charge density is mostly localized. An exception to this behavior is represented by benzene, where the maximum of the total electric field lies in the center of the molecule. The curves for tetracene and pentacene in the region above the molecule show a slight oscillation, which is due to the modulation of the charge density in that region. This effect is not observed for the smaller molecules. We verified also that, at large distances from the charge distribution, the electric field has a dipolar behavior, i.e., $E_{ind} \propto x^{-3}$ (see the SI for further details).

Figure 6 shows the enhancement of the electric field in the vicinity of the 50-acene. This result is consistent with the

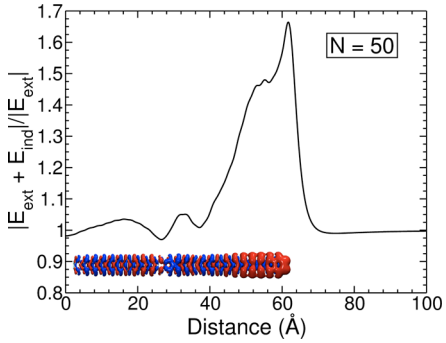

Figure 6. Electric field enhancement of longitudinally polarized excitations of the 50-acene, computed along the axis of the molecule, 3.3 Å above its plane. The distance indicated in the x axis refers to the distance from the center of the molecule, on the considered plane. The 50-acene molecule is shown in correspondence with the electric field plot.

general trend: due to the length of the molecule, the field amplification is lower than for shorter polyacenes (note the different scale on the y axis in Figure 5c and Figure 6). The effect of the modulation of the charge density response is also present, resulting in spatial oscillation of the field intensity. This is particularly evident at about one-fourth of the molecule length, where the response charge has a minimum (Figure 4). In a similar way, at the edge of the molecule, where the response charge accumulates, E_{ind} has a maximum (Figure 6).

The absolute values obtained for the electric field enhancement depend critically on the parameter of the broadening Γ in the calculation of the response charge density.[50] Here, we adopted Γ = 14 meV in calculations concerning all the molecules in order to obtain consistent results. The comparison with results obtained using different values of this parameter should be done keeping in mind its influence. To check this point, we calculated E_{ind} using different values of Γ, and we found that its modulus is proportional to the inverse of this parameter, $E_{ind} \propto \Gamma^{-1}$. This result gives also an ab initio validation of previous results on graphene nanoflakes[50] obtained from a simplified approach.

On the basis of the fast spatial decay of the induced electric fields, we conclude that the field enhancement provided by polyacenes is not what is needed for realistic applications of these systems as single-molecule amplifiers. Further strategies have to be considered to use C-based nanostructures as nanoantennas.

Effect of Coupling Molecular Excitations: The Naphthalene Dimer. In order to elucidate a possible strategy to improve the field enhancement in this class of systems, we considered, as a proof of concept, the effect of the cooperative interaction between polyacenes. In particular, we considered a dimer composed of two naphthalene molecules aligned as shown in Figure 7a, and we studied the changing of the optical properties as a function of the intermolecular distance d, defined as the distance between the two nearest hydrogen atoms belonging to different molecules.

The absorption spectra of dimers with increasing distance are shown in Figure 7b, where we observe an evident change in the energy position of the main β peak around 5.5 eV. The energy position of the small p peak at lower energy (~4.0 eV) remains, instead, essentially unchanged.

This behavior is analyzed more deeply by plotting the energy and the intensity of the β peak as a function of the intermolecular distance (Figure7c,d respectively). We report the analogous intensity of the low-intensity peak p in the SI. Figure 7c shows that the energy of the β peak of the naphthalene dimer increases monotonically when the distance between the two molecules is increased, approaching asymptotically the value of the isolated molecule. The excitation energy shift for long distances is expected to decay as d^{-3},[81] a trend that we indeed recover.

The intensity has a maximum for d = 2.18 Å (Figure 7d), then it decreases monotonically. For the largest d considered here, 7.62 Å, the intensity value is still greater than 2 times that of the single molecule. This shows the importance and the relative long-range nature of the mutual polarization of the molecules. In fact, for simplistic two-level molecules (i.e., molecules with no intrinsic polarizability besides that due to the studied transition), the expected absorption intensity would be just twice that of the isolated molecule. This trend is particularly interesting in view of the "plasmonic" response behavior of the system.

Figure 8 shows the electric field enhancement produced by the excitation of the β peak of the naphthalene dimer, computed along the long axis connecting the two molecules, in the same geometrical condition as before. The trend of the total electric field in the vicinity of the naphthalene dimer is qualitatively in agreement with the electric field produced by two finite size dipoles that oscillate in phase (see the SI for further details), being characterized by two peaks of different intensities, one in correspondence with the edges of each molecule. The higher peak is always that located on the edge farthest from the other molecule, again in agreement with the simple finite size dipolar model in the SI. For the systems with a small distance between the naphthalenes, the two peaks become a single peak with a smaller shoulder. The maximum enhancement is not a monotonic function of the distance, and it peaks for d = 5.92 Å and for d = 2.86 Å. For these distances, the enhancement is around 12, to be compared with 9 for the

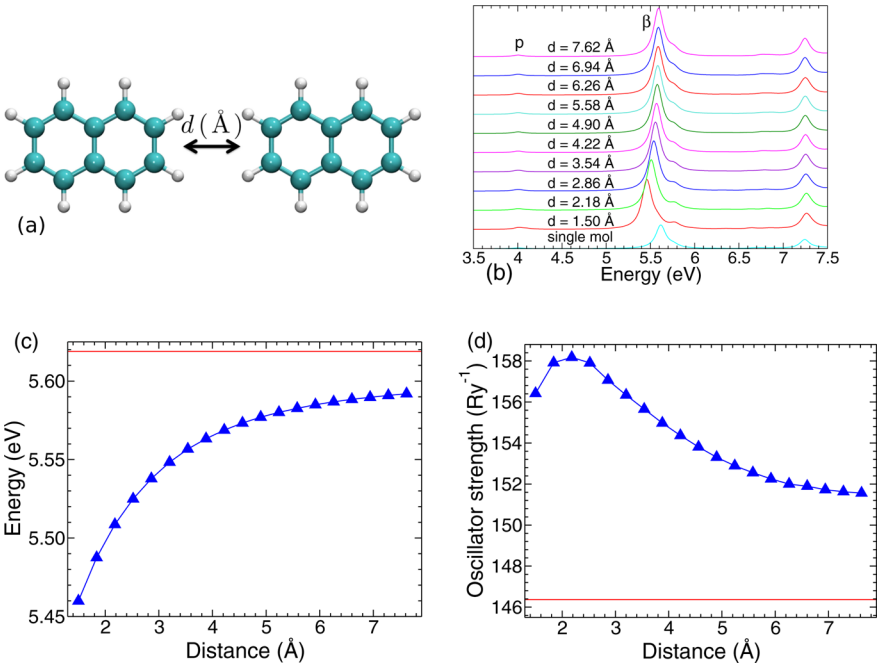

Figure 7. Naphthalene dimer. (a) Representation of the configuration of the naphthalene dimer. (b) Absorption spectra in the low-energy region with increasing distance d between molecules. Energy position (c) and intensity (d) of the main absorption peak β of the dimer as a function of the distance d. The red lines indicate the energy of the β peak for the single naphthalene molecule in panel c and the intensity of the β peak for the single naphthalene molecule multiplied by a factor 2, in panel d.

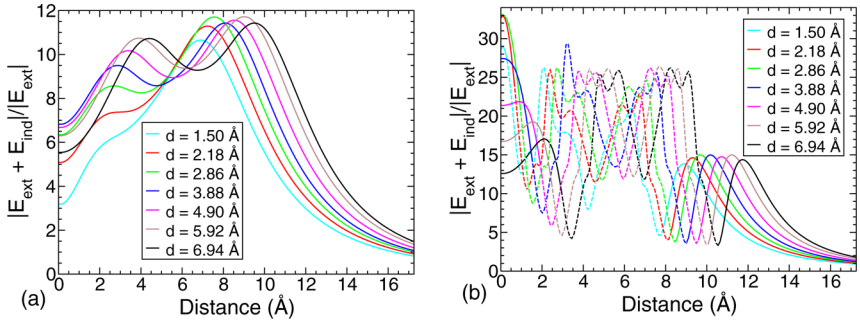

Figure 8. Electric field enhancement of longitudinally polarized excitations of the naphthalene dimer, for different intermolecular distances (d), (a) computed along the long axis of the molecules, 3.3 Å above its plane, and (b) on the plane of the molecules. The distance indicated in the x axis refers to the distance from the center of the dimer, on the considered plane. In panel b, the electric field enhancement calculated in the area occupied by one molecule, where the electric field is unphysical, is depicted with a dashed line.

single molecule, i.e., +33%. Larger improvements are obtained when the electric field is calculated in the space separating the two molecular edges. In this case, for d = 6.94 Å, which could accommodate a third, small, molecule in between the two naphthalenes, the enhancement is comprised between 12 and 17, up to ∼90% larger than for single molecules (Figure 8b). Even larger enhancements are obtained for smaller d, which however may accommodate only a few atoms. While the improvement with respect to the single acene is not spectacular in absolute value, these examples suggest that a proper supramolecular arrangement of a C-based system may enhance the field amplification factor of the system in a simple and predictable way, paving the way for more realistic "molecular-plasmonic" applications.

CONCLUSIONS

In this work we presented a *bottom-up* study of the electronic and optical absorption properties of polyacenes of different length, which represent a molecular limit of graphene nanostructures. Then we extended the analysis to the case of a naphthalene dimer, a prototypical example of molecular assembly. We have shown that the acenes exhibit a large dipolar optical excitation, interpretable as a *molecular plasmon*, upon the application of an oscillating electric field (i.e., incoming light) along the direction of the molecular axis. Our analysis focused on the achievable enhancement of such an external electric field, in resonance condition with the molecular excitation.

The resulting confinement of electromagnetic energy to nanometric regions can produce a local enhancement of the external electromagnetic field near the nanosystem, thus acting as an optical plasmonic nanoantenna. In the present case, the amplification of the electric field in the vicinity of acenes is rather small and decreases when the size of the system is increased. We have thus investigated a dimer of acenes, showing that enhancement can be improved. This result paves the way for the design of more complex C-based architectures, explicitly conceived to enhance the amplification factor.

dx.doi.org/10.1021/ph500269q | ACS Photonics 2014, 1, 1049−1058

Finally, this work emphasizes that the use of first-principles methods, such as the TDDFT approach adopted here, is required to correctly describe optical and plasmonic properties of nanoscale systems.

■ ASSOCIATED CONTENT

Supporting Information

The SI includes details on ground and excited states of short acenes and the corresponding response charge plots and electric field behaviors. An mpg movie of time-oscillating response charge is also included. This material is available free of charge via the Internet at http://pubs.acs.org.

■ AUTHOR INFORMATION

Corresponding Authors

*E-mail: arrigo.calzolari@nano.cnr.it.
*E-mail: stefano.corni@nano.cnr.it.

Notes

The authors declare no competing financial interest.

■ ACKNOWLEDGMENTS

Computer resources were provided by the CINECA supercomputing center at their Fermi BG/Q machine through the ISCRA_C project. We would like to thank Caterina Cocchi for useful discussions. Rita Stacchezzini provided valuable graphical aid. This work was supported by MIUR through the program "Progetto Premiale 2012" - Project ABNANOTECH and through Project PRIN Contract No. 2008525SC7.

■ REFERENCES

(1) Tame, M. S.; McEnery, K. R.; Özdemir, Ş. K.; Lee, J.; Maier, S. A.; Kim, M. S. Quantum plasmonics. *Nat. Phys.* **2013**, *9*, 329−340.

(2) Giannini, V.; Fernández-Domínguez, A. I.; Heck, S. C.; Maier, S. A. Plasmonic nanoantennas: fundamentals and their use in controlling the radiative properties of nanoemitters. *Chem. Rev.* **2011**, *111*, 3888−3912.

(3) Berweger, S.; Atkin, J. M.; Olmon, R. L.; Raschke, M. B. Light on the tip of a needle: plasmonic nanofocusing for spectrometry on the nanoscale. *J. Phys. Chem. Lett.* **2012**, *3*, 945−952.

(4) García de Abajo, F. J. Optical excitations in electron microscopy. *Rev. Mod. Phys.* **2010**, *82*, 209−275.

(5) Morton, S. M.; Silverstein, D. W.; Jensen, L. Theoretical studies of plasmonics using electronic structure methods. *Chem. Rev.* **2011**, *111*, 3962−3994.

(6) Schuller, J. A.; Barnard, E. S.; Cai, W.; Jun, Y. C.; White, J. S.; Brongersma, M. L. Plasmonics for extreme light concentration and manipulation. *Nat. Mater.* **2010**, *9*, 193−204.

(7) Nordlander, P. Molecular tuning of quantum plasmon resonances. *Science* **2014**, *343*, 1444−1445.

(8) Atwater, H. A.; Polman, A. Plasmonics for improved photovoltaic devices. *Nat. Mater.* **2010**, *9*, 205−213.

(9) Thomann, I.; Pinaud, B. A.; Chen, Z.; Clemens, B. M.; Jaramillo, T. F.; Brongersma, M. L. Plasmon enhanced solar-to-fuel energy conversion. *Nano Lett.* **2011**, *11*, 3440−3446.

(10) Noginov, M. A.; Gu, L.; Livenere, J.; Zhu, G.; Pradhan, A. K.; Mundle, R.; Bahoura, M.; Barnakov, Y. A.; Podolskiy, V. A. Transparent conductive oxides: plasmonic materials for telecom wavelengths. *Appl. Phys. Lett.* **2011**, *99*, 021101.

(11) Pelton, M.; Aizpurua, J.; Bryant, G. Metal-nanoparticle plasmonics. *Laser Photonics Rev.* **2008**, *2*, 136−159.

(12) Anker, J. N.; Hall, W. P.; Lyandres, O.; Shah, N. C.; Zhao, J.; Van Duyne, R. P. Biosensing with plasmonic nanosensors. *Nat. Mater.* **2008**, *7*, 442−453.

(13) Jeanmaire, D. L.; Van Duyne, R. P. Surface Raman spectroelectrochemistry: Part I. Heterocyclic, aromatic, and aliphatic amines adsorbed on the anodized silver electrode. *J. Electroanal. Chem. Interfacial Electrochem.* **1977**, *84*, 1−20.

(14) Juluri, B. K.; Lu, M.; Zheng, Y. B.; Huang, T. J.; Jensen, L. Coupling between molecular and plasmonic resonances: effect of molecular absorbance. *J. Phys. Chem. C* **2009**, *113*, 18499−18503.

(15) Halas, N. J.; Moskovits, M. Surface-enhanced Raman spectroscopy: substrates and materials for research and applications. *MRS Bull.* **2013**, *38*, 607−611.

(16) Kneipp, K.; Wang, Y.; Kneipp, H.; Perelman, L. T.; Itzkan, I.; Dasari, R. R.; Feld, M. S. Single molecule detection using surface-enhanced Raman scattering (SERS). *Phys. Rev. Lett.* **1997**, *78*, 1667−1670.

(17) Nie, S.; Emory, S. R. Probing single molecules and single nanoparticles by surface-enhanced Raman scattering. *Science* **1997**, *275*, 1102−1106.

(18) Ozbay, E. Plasmonics: merging photonics and electronics at nanoscale dimensions. *Science* **2006**, *311*, 189−193.

(19) Engheta, N. Circuits with light at nanoscales: optical nanocircuits inspired by metamaterials. *Science* **2007**, *317*, 1698−1702.

(20) Brongersma, M. L.; Shalaev, V. M. The case for plasmonics. *Science* **2010**, *328*, 440−441.

(21) Gramotnev, D. K.; Bozhevolnyi, S. I. Plasmonics beyond the diffraction limit. *Nat. Photonics* **2010**, *4*, 83−91.

(22) Jacob, Z.; Shalaev, V. M. Plasmonics goes quantum. *Science* **2011**, *334*, 463−464.

(23) Hunt, L. B. The true story of Purple of Cassius. *Gold Bull.* **1976**, *9*, 134−139.

(24) Wooten, F. *Optical Properties of Solids*; Academic Press, Inc.: San Diego, CA, 1972.

(25) Kreibig, U.; Vollmer, M. *Optical Properties of Metal Clusters* (Springer series in material science; v. 25); Springer-Verlag: Berlin, 1995.

(26) Della Sala, F.; D'Agostino, S. *Handbook of Molecular Plasmonics*; Pan Stanford Publishing Pte. Ltd., 2013.

(27) Aikens, C. M.; Li, S.; Schatz, G. C. From discrete electronic states to plasmons: TDDFT optical absorption properties of Ag_n (n = 10, 20, 35, 56, 84, 120) tetrahedral clusters. *J. Phys. Chem. C* **2008**, *112*, 11272−11279.

(28) Guidez, E. B.; Aikens, C. M. Diameter dependence of the excitation spectra of silver and gold nanorods. *J. Phys. Chem. C* **2013**, *117*, 12325−12336.

(29) Barcaro, G.; Sementa, L.; Fortunelli, A.; Stener, M. Optical properties of silver nanoshells from time-dependent density functional theory calculations. *J. Phys. Chem. C* **2014**, *118*, 12450−12458.

(30) Sakko, A.; Rossi, T. P.; Enkovaara, J.; Nieminen, R. M. Atomistic approach for simulating plasmons in nanostructures. *Appl. Phys. A: Mater.* **2014**, *115*, 427−431.

(31) Bernadotte, S.; Evers, F.; Jacob, C. R. Plasmons in molecules. *J. Phys. Chem. C* **2013**, *117*, 1863−1878.

(32) Townsend, E.; Bryant, G. W. Plasmonic properties of metallic nanoparticles: the effects of size quantization. *Nano Lett.* **2012**, *12*, 429−434.

(33) Malola, S.; Lehtovaara, L.; Enkovaara, J.; Häkkinen, H. Birth of the localized surface plasmon resonance in monolayer-protected gold nanoclusters. *ACS Nano* **2013**, *7*, 10263−10270.

(34) Gao, B.; Ruud, K.; Luo, Y. Shape-dependent electronic excitations in metallic chains. *J. Phys. Chem. C* **2014**, *118*, 13059−13069.

(35) Ding, F.; Guidez, E. B.; Aikens, C. M.; Li, X. Quantum coherent plasmon in silver nanowires: a real-time TDDFT study. *J. Chem. Phys.* **2014**, *140*, 244705.

(36) Guidez, E. B.; Aikens, C. M. Plasmon resonance analysis with configuration interaction. *Phys. Chem. Chem. Phys.* **2014**, *16*, 15501−15509.

(37) Jablan, M.; Buljan, H.; Soljačić, M. Plasmonics in graphene at infrared frequencies. *Phys. Rev. B* **2009**, *80*, 245435.

(38) Koppens, F. H. L.; Chang, D. E.; García de Abajo, F. J. Graphene plasmonics: a platform for strong light-matter interactions. *Nano Lett.* **2011**, *11*, 3370−3377.

(39) Christensen, J.; Manjavacas, A.; Thongrattanasiri, S.; Koppens, F. H. L.; García de Abajo, F. J. Graphene plasmon waveguiding and hybridization in individual and paired nanoribbons. *ACS Nano* **2012**, *6*, 431−440.
(40) García de Abajo, F. J. Graphene plasmonics: challenges and opportunities. *ACS Photonics* **2014**, *1*, 135−152.
(41) Gaudreau, L.; Tielrooij, K. J.; Prawiroatmodjo, G. E. D. K.; Osmond, J.; García de Abajo, F. J.; Koppens, F. H. L. Universal distance-scaling of nonradiative energy transfer to graphene. *Nano Lett.* **2013**, *13*, 2030−2035.
(42) Wang, B. J.; Ke, S. H.; Lin, H. Q. Regular quantum plasmons in segments of graphene nanoribbons. *arXiv:1308.3464*, 2013, 1−5.
(43) García de Abajo, F. J. Graphene nanophotonics. *Science (New York, N.Y.)* **2013**, *339*, 917−918.
(44) Eberlein, T.; Bangert, U.; Nair, R. R.; Jones, R.; Gass, M.; Bleloch, A. L.; Novoselov, K. S.; Geim, A.; Briddon, P. R. Plasmon spectroscopy of free-standing graphene films. *Phys. Rev. B* **2008**, *77*, 233406.
(45) Brar, V. W.; Wickenburg, S.; Panlasigui, M.; Park, C.-H.; Wehling, T. O.; Zhang, Y.; Decker, R.; Girit, Ç.; Balatsky, A. V.; Louie, S. G.; Zettl, A.; Crommie, M. F. Observation of carrier-density-dependent many-body effects in graphene via tunneling spectroscopy. *Phys. Rev. Lett.* **2010**, *104*, 036805 (1−4).
(46) Fei, Z.; et al. Infrared nanoscopy of Dirac plasmons at the graphene-SiO_2 interface. *Nano Lett.* **2011**, *11*, 4701−4705.
(47) Chen, J.; Badioli, M.; Alonso-González, P.; Thongrattanasiri, S.; Huth, F.; Osmond, J.; Spasenović, M.; Centeno, A.; Pesquera, A.; Godignon, P.; Zurutuza Elorza, A.; Camara, N.; García de Abajo, F. J.; Hillenbrand, R.; Koppens, F. H. L. Optical nano-imaging of gate-tunable graphene plasmons. *Nature* **2012**, *487*, 77−81.
(48) Alonso-González, P.; Nikitin, A. Y.; Golmar, F.; Centeno, A.; Pesquera, A.; Vélez, S.; Chen, J.; Navickaite, G.; Koppens, F. H. L.; Zurutuza Elorza, A.; Casanova, F.; Hueso, L. E.; Hillenbrand, R. Controlling graphene plasmons with resonant metal antennas and spatial conductivity patterns. *Science* **2014**, *344*, 1369−1373.
(49) Castro Neto, A. H.; Guinea, F.; Peres, N. M. R.; Novoselov, K. S.; Geim, A. K. The electronic properties of graphene. *Rev. Mod. Phys.* **2009**, *81*, 109−162.
(50) Cocchi, C.; Prezzi, D.; Ruini, A.; Benassi, E.; Caldas, M. J.; Corni, S.; Molinari, E. Optical excitations and field enhancement in short graphene nanoribbons. *J. Phys. Chem. Lett.* **2012**, *3*, 924−929.
(51) Thongrattanasiri, S.; Manjavacas, A.; García de Abajo, F. J. Quantum finite-size effects in graphene plasmons. *ACS Nano* **2012**, *6*, 1766−1775.
(52) Manjavacas, A.; Marchesin, F.; Thongrattanasiri, S.; Koval, P.; Nordlander, P.; Sánchez-Portal, D.; García de Abajo, F. J. Tunable molecular plasmons in polycyclic aromatic hydrocarbons. *ACS Nano* **2013**, *7*, 3635−3643.
(53) Guidez, E. B.; Aikens, C. M. Origin and TDDFT benchmarking of the plasmon resonance in acenes. *J. Phys. Chem. C* **2013**, *117*, 21466−21475.
(54) Clar, E. *Polycyclic Hydrocarbons*; Academic Press: London, 1964; Vol. *1, 2*.
(55) Rehwagen, M.; Müller, A.; Massolo, L.; Herbarth, O.; Ronco, A. Polycyclic aromatic hydrocarbons associated with particles in ambient air from urban and industrial areas. *Sci. Total Environ.* **2005**, *348*, 199−210.
(56) Luch, A. *The Carcinogenic Effects of Polycyclic Aromatic Hidrocarbons*; Imperial College Press: London, 2005.
(57) Malloci, G.; Mulas, G.; Joblin, C. Electronic absorption spectra of PAHs up to vacuum UV towards a detailed model of interstellar PAH photophysics. *Astron. Astrophys.* **2004**, *426*, 105−117.
(58) Tielens, A. G. G. M. *The Physics and Chemistry of the Interstellar Medium*; Cambridge University Press: Cambridge, 2005.
(59) Mattioda, A. L.; Hudgins, D. M.; Allamandola, L. J. Experimental near-infrared spectroscopy of polycyclic aromatic hydrocarbons between 0.7 and 2.5 μm. *Astrophys. J.* **2005**, *629*, 1188−1210.
(60) Ricca, A.; Bauschlicher, C. W.; Boersma, C.; Tielens, A. G. G. M.; Allamandola, L. J. The infrared spectroscopy of compact polycyclic aromatic hydrocarbons containing up to 384 carbons. *Astrophys. J.* **2012**, *754*, 75.
(61) Anthony, J. E. Functionalized acenes and heteroacenes for organic electronics. *Chem. Rev.* **2006**, *106*, 5028−5048.
(62) Anthony, J. E. The larger acenes: versatile organic semiconductors. *Angew. Chem., Int. Ed.* **2008**, *47*, 452−483.
(63) Wu, J.; Pisula, W.; Müllen, K. Graphenes as potential material for electronics. *Chem. Rev.* **2007**, *107*, 718−747.
(64) Jiang, D.-E.; Dai, S. Circumacenes versus periacenes: HOMO-LUMO gap and transition from nonmagnetic to magnetic ground state with size. *Chem. Phys. Lett.* **2008**, *466*, 72−75.
(65) Sony, P.; Shukla, A. Large-scale correlated calculations of linear optical absorption and low-lying excited states of polyacenes: Pariser-Parr-Pople Hamiltonian. *Phys. Rev. B* **2007**, *75*, 155208.
(66) Wong, B. M.; Hsieh, T. H. Optoelectronic and excitonic properties of oligoacenes: substantial improvements from range-separated time-dependent density functional theory. *J. Chem. Theory Comput.* **2010**, *6*, 3704−3712.
(67) Kronik, L.; Stein, T.; Refaely-Abramson, S.; Baer, R. Excitation gaps of finite-sized systems from optimally tuned range-separated hybrid functionals. *J. Chem. Theory Comput.* **2012**, *8*, 1515−1531.
(68) Malloci, G.; Cappellini, G.; Mulas, G.; Mattoni, A. Electronic and optical properties of families of polycyclic aromatic hydrocarbons: a systematic (time-dependent) density functional theory study. *Chem. Phys.* **2011**, *384*, 19−27.
(69) Lopata, K.; Reslan, R.; Kowalska, M.; Neuhauser, D.; Govind, N.; Kowalski, K. Excited-state studies of polyacenes: a comparative picture using EOMCCSD, CR-EOMCCSD(T), range-separated (LR/RT)-TDDFT, TD-PM3, and TD-ZINDO. *J. Chem. Theory Comput.* **2011**, *7*, 3686−3693.
(70) Giannozzi, P.; et al. QUANTUM ESPRESSO: a modular and open-source software project for quantum simulations of materials. *J. Phys.: Condens. Matter* **2009**, *21*, 395502 (1−19).
(71) Malcioğlu, O. B.; Gebauer, R.; Rocca, D.; Baroni, S. TurboTDDFT - a code for the simulation of molecular spectra using the Liouville-Lanczos approach to time-dependent density-functional perturbation theory. *Comput. Phys. Commun.* **2011**, *182*, 1744−1754.
(72) Perdew, J. P.; Burke, K.; Ernzerhof, M. Generalized gradient approximation made simple. *Phys. Rev. Lett.* **1996**, *77*, 3865−3868.
(73) Bendikov, M.; Duong, H. M.; Starkey, K.; Houk, K. N.; Carter, E. A.; Wudl, F. Oligoacenes: theoretical prediction of open-shell singlet diradical ground states. *J. Am. Chem. Soc.* **2004**, *126*, 7416−7417.
(74) Bettinger, H. F. Electronic structure of higher acenes and polyacene: the perspective developed by theoretical analyses. *Pure Appl. Chem.* **2010**, *82*, 905−915.
(75) Atkins, P.; Friedman, R. *Molecular Quantum Mechanics*, 5th ed.; Oxford University Press Inc.: New York, 2011; pp 276−281.
(76) In the plot of the DOS spectra, because of the Gaussian broadening of the states we use, states very close to each other may result in a superposition, which is a graphic effect and does not affect the corresponding optical properties.
(77) Karcher, W.; Fordham, R.; Dubois, J.; Glaude, P.; Ligthart, J. *Spectral Atlas of Polycyclic Aromatic Compounds*; Springer: New York, 1985.
(78) Ge, X.; Binnie, S. J.; Rocca, D.; Gebauer, R.; Baroni, S. turboTDDFT 2.0 - hybrid functionals and new algorithms within time-dependent density-functional perturbation theory. *Comput. Phys. Commun.* **2014**, *185*, 2080−2089.
(79) van Faassen, M.; de Boeij, P. L.; van Leeuwen, R.; Berger, J. A.; Snijders, J. G. Ultranonlocality in time-dependent current-density-functional theory: application to conjugated polymers. *Phys. Rev. Lett.* **2002**, *88*, 186401 (1−4).
(80) Charaf-Eddin, A.; Planchat, A.; Mennucci, B.; Adamo, C.; Jacquemin, D. Choosing a functional for computing absorption and

fluorescence band shapes with TD-DFT. *J. Chem. Theory Comput.* **2013**, *9*, 2749−2760.
(81) Craig, D. P.; Thirunamachandran, T. *Molecular Quantum Electrodynamics, An Introduction to Radiation-Molecule Interaction*; Academic Press Inc.: London, 1984.